Extension and validation of aerosol wash-down model on inclined wall

Fangnian Wang *, Xu Cheng

Institute for Applied Thermofluidics (IATF), Karlsruhe Institute of Technology (KIT), Kaiserstraße 12, Karlsruhe 76131, Germany

ARTICLE INFO

Keywords:
Aerosol wash-down
Condensate coverage
Rivulet
Inclination
Cohesion
Particle erosion

ABSTRACT

During severe accidents, fission products as aerosols are released into the containment and consequently deposited on walls. The condensate flow on walls could wash the deposited aerosols downwards to the sump. The aerosol wash-down process on walls is significant to evaluate radiative source term distribution in nuclear containment. In this paper, the aerosol wash-down model **AULA** is extended to be valid for inclined walls and cohesive aerosols. Moreover, the condensate coverage is coupled to calculate the aerosol mass washed down by the condensate flow. A correlation of condensate coverage is proposed and validated against experimental data. In order to improve the dimensionless critical shear stress model, a correction factor, which considers wall inclination and aerosol cohesion, is deduced by the force analysis. The extended aerosol wash-down model is validated against the THAI-AW3-LAB experiment. The results comparison show generally good agreements. Furthermore, the model characteristics under severe accident conditions and the analyses on parameters, such as aerosol density, diameter, and inclination are presented and discussed.

1. Introduction

During severe accidents, fission products are generated due to core degradation in reactor pressure vessel and molten core-concrete interactions outside reactor vessel, and released into the containment with large amount of steam and non-condensable gases. Together with the steam condensation, aerosols are transferred into the wall (Weber et al., 2015). The condensate flow washes down the aerosols, and transports them into lower compartments or sumps. This aerosol wash-down process governs the distribution of the fission products. Fission products in the water produce steam due to the decay heat as well as decay heat released on dry structures causes a dry heating. Furthermore, source term distribution is important to assess radiation damages of local components like electronic devices, seals, etc.

The aerosol wash-down process interacts with thermal-hydraulics and aerosol particle transportation process in the containment (Weber et al., 2015). Under different severe accident scenarios, there are different trends of containment thermal-hydraulics, aerosol properties, aerosol injection, etc. The containment thermal-hydraulics, e.g. the gas and wall temperature, and condensate flow rate strongly influence the condensate coverage, namely the water-covered area fraction on surface. The aerosol injection is affected by core damage process and molten core-concrete interaction, which is the source term of aerosol deposition and wash-down process on surfaces.

In the **CO**ntainment **CO**de **SYS**tem COCOSYS, the thermal-hydraulics and the aerosol wash-down process are modelled (Klein-Heßling et al., 2015). For instance, the aerosol wash-down model for insoluble aerosols **AULA** (German: "**A**bwaschen **u**n**l**öslicher **A**erosole") simulates the erosion of insoluble aerosols by flowing condensate. The erosion takes place if the flow shear velocity at the wall exceeds the critical threshold (Shields' criterion in sediment transport theory (Guo, 2002)). However, the condensate coverage is an important parameter that indicates how much wetted area the aerosol wash-down takes place. The condensate coverage is considered empirically as rivulets with a user given value in COCOSYS. Our previous investigation shows the condensate coverage depends on the volume flow rate per width, contact angles, surface inclination, and fluid properties (Wang and Cheng, 2019).

2. Aerosol wash-down model

The aerosol wash-down processes for soluble and insoluble aerosols are quite different. **Soluble aerosols**, like CsI, are quickly dissolved and transported with the flow. The dilution process is simplified to assume an instantaneous and complete dissolution of wetted particles. The wash-down efficiency is dominated by the condensate coverage. The model in COCOSYS for soluble aerosols was successfully validated on experiments THAI-AW and THAI-AW2 (Hoehne and Weber, 2010). THAI-AW experiment

* Corresponding author.
E-mail address: fangnian.wang@kit.edu (F. Wang).

Nomenclature

A	wall area, m^2
A_H	Hamaker constant,$A_H \cong 10^{-20}$ Joule
$C_{i,c}$	correction factor of inclination and cohesion
c_{ae}	deposited aerosols load on surface, kg/m^2
$c_{ae,0}$	initial deposited aerosols load on surface, kg/m^2
c_δ	prefactor of empirical rivulet thickness correlation
d_p	particle diameter, m
F_C	cohesive force, N
F_D	drag force of the overlying flow, N
F_L	lift force of the overlying flow, N
F_W	buoyant weight of particle, N
g	gravity acceleration,$9.8 m/s^2$
Ka	Kapitza number
$K(n)$	compaction function of particle
$k_{D,1}$	constant factors of drag force (as well as $k_{D,2}$)
k_e	erosion rate, 1/s
$k_{e,0}$	erosion constant, 1/s
k_L	constant factors of lift force
k_W	constant factors of buoyant weight force
m_{ae}	remaining deposited aerosol mass on water-covered area, kg
n	porosity of particles
R^*	dimensionless auxiliary parameter
Re	Reynolds number
Re^*	particle Reynolds number
s	density ratio of particle to water
t	time, s
u	rivulet (condensate) velocity, m/s
u^*	rivulet (condensate) shear velocity, m/s
u_c^*	critical shear velocity of particle, m/s
$\dot{V}$	volume flow rate per width, $m^3/(m{\cdot}s)$

Greek symbols

α	inclination angle, °
α_c	characteristic internal friction angle (critical inclination angle), °
δ	rivulet (condensate) thickness, m
ε	rivulet (condensate) coverage
$\theta_{s,A}/\theta_{s,R}$	static advancing and receding contact angle, °
θ_e	equilibrium contact angle, °
μ	water viscosity, Pa·s
μ_c	Coulomb friction coefficient
ν	kinematic viscosity, m^2/s
π	dimensionless number, π_1-π_5
ρ	water density, kg/m^3
σ_{LG}	surface tension between water and air, N/m
τ_c	critical shear stress, Pa
τ_c^*	dimensionless critical shear stress
$\tau_{c,o}^*$	dimensionless critical shear stress of horizontal bed

investigated the wash-down behavior of soluble CsI aerosol deposited over surfaces (Gupta and Langer, 2009). THAI-AW2 experiment was performed subsequently to investigate the wash-down behavior of both soluble CsI aerosol and insoluble SnO_2 aerosol from vertical walls and quasi-horizontal surfaces by steam condensate (Gupta et al., 2012).

However, the wash-down of **insoluble aerosols,** like Ag and AgO_x aerosols, are more complex because the wash-down process depends on the particle properties (size and density), particle porosity, surface inclination (wall and floor), thermal–hydraulic conditions (flow patterns, condensate coverage, and fluid properties), etc.

The aerosol wash-down model AULA (Weber, 2011; Weber et al., 2015) is based on an approach used in geology to describe the transport of sediments in water flow. The Shields criterion (Shields, 1936) is adopted in AULA, which states that particles erode if the flow shear velocity exceeds the critical shear velocity determined by particles. The AULA model suggests the surface load (surface density) (called 'concentration' in Weber et al., 2015) of deposited aerosols on walls c_{ae}, kg/m^2, decreases as an exponential function:

$$\frac{dc_{ae}}{dt} = -k_e \cdot c_{ae} \tag{1}$$

where k_e, 1/s, is the erosion rate, i.e. the characteristic time of the erosion process, which has to be measured for each specific condition. The aerosol mass erosion rate k_e for cohesive particles is introduced by (Ariathurai, 1977):

$$k_e = \begin{cases} k_{e,0}\left(\frac{u^{*2}-u_c^{*2}}{u_c^{*2}}\right), u^* > u_c^* \\ 0, u^* \le u_c^* \end{cases} \tag{2}$$

where $k_{e,0}$ is an erosion constant that has to be estimated. This constant depends on the aerosol particle and flow properties (Weber et al., 2015; Amend et al., 2018). According to the Shields criterion, the erosion of particles takes place if the flow shear velocity u^* is beyond the critical shear velocity u_c^* of particle; otherwise, there is no erosion.

The critical shear velocity of particle is:

$$u_c^* = \sqrt{\tau_c/\rho} = \sqrt{\tau_c^*(s-1)gd_p} \tag{3}$$

where τ_c is the critical shear stress and ρ is the water density. The definition of critical Shields parameter, namely the dimensionless critical shear stress, is:

$$\tau_c^* = \frac{\tau_c}{(s-1)\rho g d_p} \tag{4}$$

where d_p is the particle diameter and g is the gravity acceleration. The density ratio s of particle to water is defined as:

$$s = \rho_p/\rho \tag{5}$$

In AULA, an empirical correlation of the horizontal and non-cohesive particle bed (Guo, 2002) is applied. This empirical correlation is fully validated for a large range of particle size and flow velocity. The empirical critical Shields parameter, namely dimensionless critical shear stress of horizontal particle bed, is:

$$\tau_{c,o}^* = 0.1(R^*)^{\frac{2}{3}} + 0.054\left[1 - e^{\left(-0.1(R^*)^{\frac{2}{3}}\right)}\right] \tag{6}$$

where the dimensionless auxiliary parameter R^* is:

$$R^* = \frac{d_p\sqrt{0.1(s-1)gd_p}}{\nu} \tag{7}$$

where ν is the kinematic viscosity of water.

The deduction of the shear velocity u^* depends on the type of flow. Due to the slight roughness of the decontamination paint surface (a typical structure surface in containment), smooth turbulent flows can be expected (Weber et al., 2015). The shear velocity of

hydraulically smooth flow is calculated by using a parabolic flow velocity profile (Hillebrand, 2008).

$$u^* = u\frac{0.41}{ln\left(\frac{u^*\delta}{\nu}\right)+5.25} \tag{8}$$

where u and δ are the condensate (e.g. rivulet, film) velocity and thickness respectively. The Karman constant is 0.41. The integration constant is in the range of [5.0, 5.5]. Here the average integration constant of 5.25 is adopted. The u^* can be solved by the iteration of the implicit Eq. (8). It should be pointed out that, for the rough surface in containment, the roughness of the structure has to be introduced to calculate the shear velocity (Hillebrand, 2008).

The integral form of the surface load of deposited aerosols c_{ae} can be obtained by Eq. (1). The remaining deposited aerosol mass on water-covered area is:

$$m_{ae} = A\cdot\varepsilon\cdot c_{ae,0}\cdot e^{(\ k_e t)} \tag{9}$$

where A is the area of the whole wall, and ε is the condensate coverage. $c_{ae,0}$, kg/m^2, is the initial surface load of deposited aerosols. Since the condensate coverage ε in AULA is a user given value, in this paper, a condensate coverage correlation will be proposed, and then coupled into the aerosol wash-down mass calculation.

Moreover, inclined walls usually exist in nuclear containment, and the experiments (e.g. THAI-AW3-LAB) reveal that the cohesive force cannot be neglected for the nuclear aerosols deposited on inclined surfaces (Laufenberg et al., 2014a,b). In AULA, the dimensionless critical shear stress of aerosols, known as the critical Shields parameter, was adopted as an empirical correlation but without the consideration of wall inclination and aerosol cohesion. Therefore, in this paper, a correction factor for the dimensionless critical shear stress $\tau^*_{c,o}$ of horizontal non-cohesive bed with the consideration of inclination angle and particle cohesion is introduced:

$$\tau^*_c = C_{i,c}\cdot\tau^*_{c,o} \tag{10}$$

where $C_{i,c}$ is the combined correction factor for inclination and cohesion.

Overall, the objective of this paper is to develop a condensate coverage empirical correlation and propose a correction factor of the combination of wall inclination and aerosol cohesion effects. The extended aerosol wash-down model will be validated against the THAI-AW3-LAB experimental data, and the model characteristics will be analyzed under prototypic severe accident conditions.

3. Model improvement

3.1. Condensate coverage

3.1.1. Dimensionless parameters

For the dimensional analysis, the Buckingham π theorem is applied to reduce the physical problem to the simplest (most economical) form (Bridgman, 1931; Buckingham, 1914). The first and most important step in the dimensional analysis is to identify a complete set of independent quantities. For the current case, one known is that the condensate coverage ε on inclined wall depends on the independent quantities, such as volume flow rate per width $\dot{V}$, equilibrium contact angle θ_e (which is the static equilibrium contact angle. The 'static' means the contact area between liquid and solid doesn't change during the measurement. The equilibrium contact angle can be calculated from the static advancing and static receding contact angle), inclination angle α, gravitation g, fluid density ρ, fluid dynamic viscosity μ, and surface tension σ_{LG} (Wang and Cheng, 2019), namely,

$$\varepsilon = f\left(\dot{V},\theta_e,\alpha,g,\rho,\mu,\sigma_{LG}\right) \tag{11}$$

This expression can be rewritten as a dimensionless form Eq. (12). The number of dimensionless parameters is equal to the total number of variables minus the number of physical dimensions involved. For the interested physical quantities of condensate coverage, three basic dimensions involved, which are length [m], time [s], and mass [kg], are usually taken into count. All physical quantities have dimensions, which can be expressed as products of powers of these three base dimensions. We now can define the dimensionless form with the 5 (i.e. 8–3 = 5, 5 π terms) remaining dimensionless numbers:

$$f(\pi_1,\pi_2,\pi_3,\pi_4,\pi_5) = 0 \tag{12}$$

Since the coverage ε, the equilibrium contact angle θ_e, and the inclination angle α are already dimensionless numbers, the remaining 5 quantities ($\dot{V}$, g, ρ, μ and σ_{LG}) can yield the other two dimensionless number. These 5 quantities are combined and arranged, in sequence, to find the last two π terms in simplest dimensionless form:

$$\pi_1 = \frac{\rho\dot{V}}{\mu} \tag{13}$$

$$\pi_2 = \sigma_{LG}\left(\frac{\rho}{g\mu^4}\right)^{\frac{1}{3}} \tag{14}$$

π_1 times a factor 4 is the Reynolds number $Re = \frac{4\rho\dot{V}}{\mu}$, and π_2 is exactly the Kapitza number $Ka = \sigma_{LG}\left(\frac{\rho}{g\mu^4}\right)^{1/3}$. The equilibrium contact angle θ_e and inclination angle α physically influence the surface tension force and gravitation in the forms as $(1 \quad cos\theta_e)$ and $sin\alpha$ respectively. Therefore, the coverage ε can be expressed ultimatedly as a relationship among all the π terms:

$$\varepsilon = f(Re, Ka, 1-cos\theta_e, sin\alpha) \tag{15}$$

3.1.2. Empirical condensate coverage correlation

According to our previous study (Wang and Cheng, 2019), the condensate coverage definition can be expressed as follows:

$$\varepsilon = \frac{\dot{V}}{u\cdot\delta} \tag{16}$$

It is no doubt that the flow patterns of condensate have three phases, i.e., the moving droplets, rivulets and fully covered film (Wang and Cheng, 2019). For the fully covered film, the coverage $\varepsilon = 1$ and the film velocity and thickness can be obtained from film theory (e.g. Nusselt, 1916). In case of moving droplets, the velocity distribution depends on droplet size, so that only a part of droplets is effective for aerosol wash-down. The rivulet velocity is much higher than the velocity of moving droplets. Therefore, here we suppose the rivulet flow pattern dominates the coverage when the wall is not fully covered by film.

The minimum total energy (MTE) method is wildly examined for determining the rivulet thickness of an isothermal rivulet flowing down a sloped wall. In previous research (Hartley and Murgatroyd, 1964; Hobler,1964; Doniec, 1988, 1991; El-Genk and Saber, 2001; Huang and Cheng, 2015), analytical velocity and structure expressions of a stable rivulet are developed. Summaries from the literature review reveal the empirical rivulet thickness correlation derived by the authors is:

$$\delta = c_\delta\cdot(1-cos\theta_e)^{0.2}\left[\frac{\mu^2\sigma_{LG}}{\left(\rho^3(gsin\alpha)^2\right)}\right]^{0.2} \tag{17}$$

Table 1
Prefactor c_δ of empirical rivulet thickness expression.

Reference	Hartley and Murgatroyd, 1964	Doniec, 1988, 1991	Hobler,1964
Prefactor	1.34 1.72	1.45 1.125	1.86

where c_δ is the prefactor of the empirical rivulet thickness expression, which varies in the range of (1.125–1.86), as shown in Table 1.

The rivulet velocity distribution from the wall to the rivulet interface with gas is assumed as a parabolic profile (El-Genk and Saber, 2001), so the average rivulet velocity is:

$$u = \frac{\rho g sin\alpha}{3\mu}\delta^2 \tag{18}$$

The previous research (Huang and Cheng, 2015) reveals that the main part of rivulet is a rectangular film sheet with a constant thickness. The rivulet average thickness and velocity change slightly when the rivulet width varies with the condensate flow rate. Comparing with the main part of rivulet, the proportion of the arc parts of rivulet edges are very small. Substituting the rivulet thickness and the average rivulet velocity into the coverage expression, one can be derived as follows:

$$\begin{aligned}\varepsilon &= \frac{\dot{V}}{u\cdot\delta} = \frac{\dot{V}}{\frac{\rho g sin\alpha}{3\mu}\delta^3} = \frac{\dot{V}}{\frac{\rho g sin\alpha}{3\mu}\left(c_\delta\cdot(1\ \ cos\theta_e)^{0.2}\left(\frac{\mu^2\sigma_{LG}}{\rho^3(gsin\alpha)^2}\right)^{0.2}\right)^3} \\ &= \frac{0.75}{c_\delta^3}\cdot\frac{4\rho\dot{V}}{\mu}\left(\sigma_{LG}\left(\frac{\rho}{g\mu^4}\right)^{\frac{1}{3}}\right)^{0.6}(1-cos\theta_e)^{\ 0.6}(sin\alpha)^{0.2}\end{aligned} \tag{19}$$

We substitute all the dimensionless numbers (as shown in Eq. (15)) into above Eq. (19):

$$\varepsilon = \frac{0.75}{c_\delta^3}\cdot Re^1 Ka^{\ 0.6}(1-cos\theta_e)^{\ 0.6}(sin\alpha)^{0.2} \tag{20}$$

Due to $c_\delta \in (1.125, 1.86)$, the prefactor $\frac{0.75}{c_\delta^3} \in (0.12, 0.52)$ accordingly.

In order to determine the prefactor $\frac{0.75}{c_\delta^3}$, the results of our previous work (Wang and Cheng, 2019) are applied, as shown in Fig. 1. Two cases with different surfaces are simulated: a wet surface and a dry one. The wet surface case means the structure surface is pre-wetted. The rivulet forms on the pre-wetted surface when the water is injected on the uppermost edge of test plate. On the contrary, the dry surface case means the rivulet generates on the dry surface of the test plate. These two surface conditions have different equilibrium contact angles. The equilibrium contact angle on pre-wetted surface is smaller than on dry surface.

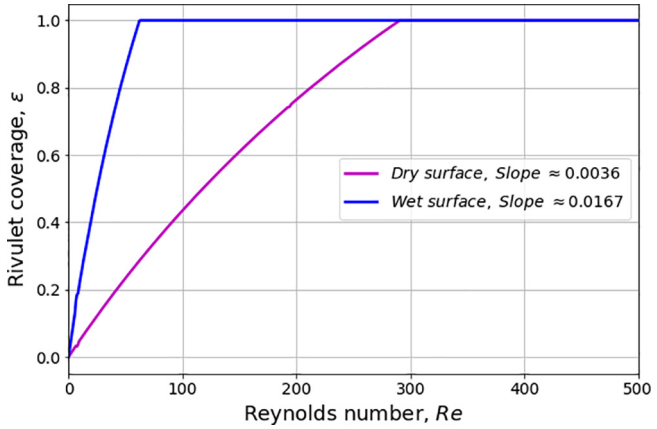

Fig. 1. Calculation results from reference (more details in Wang and Cheng, 2019, Section 3.1, Fig. 7). The boundary conditions: the equilibrium contact angles $\theta_e = 45.1A^\circ$ for dry surface and $14A^\circ$ for wet surface; the inclination angle $\alpha = 90^\circ$ for a vertical wall; the temperature and pressure are ambient.

The results reveal that the predicted relationship between the coverage and Reynolds number is almost linear, because the average rivulet thickness and velocity don't increase much when volume flow rate increases. It is consistent with the empirical correlation that the coverage is proportional toRe roughly $\varepsilon \propto Re$, if the rivulet average thickness and velocity are fixed hypothetically. According to the slopes of the curves in Fig. 1, now we can evaluate the prefactor $\frac{0.75}{c_\delta^3} \approx 0.26$, and accordingly the rivulet thickness prefactor $c_\delta = 1.424$.

Therefore, after determined the factor c_δ, the empirical condensate coverage correlation can be expressed eventually as:

$$\varepsilon = 0.26\cdot Re^1 Ka^{\ 0.6}(1-cos\theta_e)^{\ 0.6}(sin\alpha)^{0.2} \tag{21}$$

The valid parameter ranges of the condensate coverage correlation are as follows: the Kapitza number $Ka \in (2500, 22500)$, which depends on the condensate temperature and pressure inside the containment. The static equilibrium contact angle $\theta_e \in (0A^\circ, 90A^\circ)$, excluding the cases of $0A^\circ$ and $90A^\circ$. The inclination angle $\alpha \in (0A^\circ, 90A^\circ]$, excluding the horizontal surface but including the vertical. The Reynolds number is from 0 to the maximum value (when the coverage equals one).

3.1.3. Comparison with experimental data

Four experiments including 89 experimental data points from the open literatures are applied to validate the current condensate coverage model (Ausner, 2007; Yu et al., 2012; Laufenberg et al., 2014a,b; Dupont, 2017). The information of these experimental data for validation is summarized in Table 2. Actually not all contact angles are given by each individual experiment, but the surface materials are known. In Ausner experiment, the static advacing contact angle measured varies between 60° and 70° with a measurement error 6–9°. The average contact angle of 65° is adopted here. In THAI-AW3-LAB experiment, the equilibrium contact angle of water on GEHOPON paint is about 60–65°.

Fig. 2 shows the comparison between the coverage predicted by correlation Eq. (21) with the prefactor 0.26 and the experimental data. The comparison results indicate generally a good agreement with around ±25% deviation. This deviation might be caused by the surface contact angle effect, e.g. the steel plate used in the experiment of (Ausner, 2007) is a non-treated surface. The roughness of the surface is so uneven that the contact angle varies in a large range.

3.2. Correction factor of inclination and cohesion

3.2.1. Force analysis

In this section we will figure out the correction factor of the dimensionless critical shear stress τ_c^* with the consideration of inclination angle and particle cohesion, which can be obtained from the force analysis of particles.

Let us consider a particle located at the water-particle interface as presented in Fig. 3. The water-particle interface is assumed to be sloped with an inclination angle α, which is the angle between the surface and the horizontal direction. Its stability is characterized by the balance between the following forces: (1) the buoyant weight of the particle F_W, which is perpendicular to the ground without inclination, (2) the drag force of the overlying flow F_D, which is caused by the flow shear stress, and parallel to the inclined surface or the flow direction, (3) the effective cohesive force F_C, which is perpendicular to the wall surface, (4) the lift force of the overlying flow F_L, and (5) the friction force F_F of the particle in the first layer.

Table 2
Experimental data for rivulet coverage validation.

Experiment	*Re*	$\theta_{s,A}/\theta_{s,R}$	Inclination	Temperature	Data points
WEBREC	10 500	71.8A°/18.4A°	90°	Ambient	21
	20 110	18A°/10A°	90°	Ambient	15
Ausner, 2007	30 240	65A°/	60°	Ambient	43
THAI-AW3-LAB	261 285	$\theta_e = 60$ 65A°	2°,10°,20°	Ambient	6
LINX	18 62	65A°/45A°	90°	67–113 °C	4

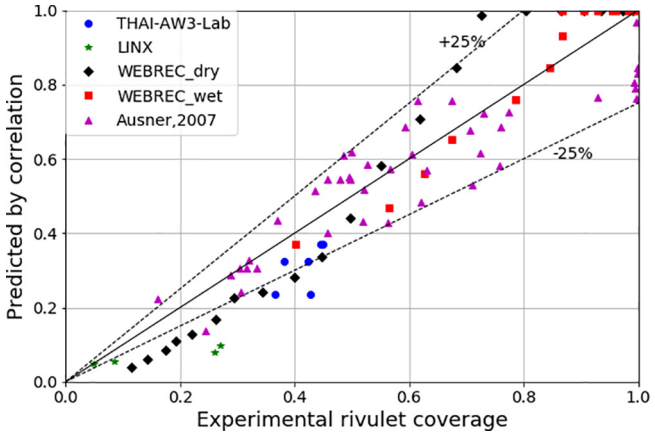

Fig. 2. Coverage comparison between correlation and experiments.

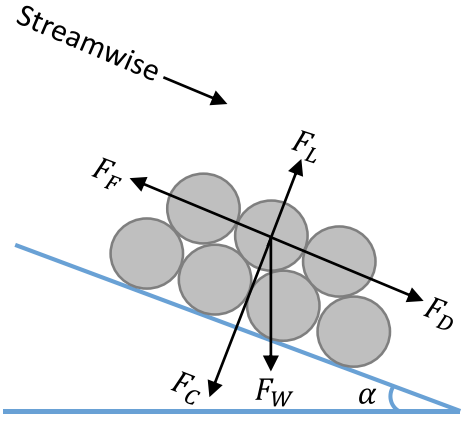

Fig. 3. Forces acting on a particle located at the water-particle interface.

The buoyant weight component $F_W cos\alpha$, F_C, and F_L are perpendicular to the surface, so that the friction force parallel to surface is:

$$F_F = \mu_c(F_W cos\alpha + F_C - F_L) \tag{22}$$

where μ_c is the Coulomb friction coefficient. The erosion criterion comes from the particle movement initiation, which usually fulfill the all external force balance at the flow direction:

$$F_D = \mu_c(F_W cos\alpha + F_C - F_L) - F_W sin\alpha \tag{23}$$

Arrange and combine the like terms:

$$F_D + \mu_c F_L = \mu_c F_W \left(cos\alpha - \frac{sin\alpha}{\mu_c} + \frac{F_C}{F_W}\right) \tag{24}$$

Substituting the following forces' expressions (Ternat et al., 2008):

$$F_W = k_W g(s-1)\rho d_p^3 \tag{25}$$

$$F_D = k_{D,1}\rho u^2 Re^{*2}\left(1 + k_{D,2}Re^{*2}\right) \tag{26}$$

$$F_L = k_L \rho u^2 Re^{*3} \tag{27}$$

into the force balance Eq. (24), yields:

$$\begin{aligned} &k_{D,1}\rho u^2 Re^{*2}\left(1 + k_{D,2}Re^{*2}\right) + \mu_c k_L \rho u^2 Re^{*3} \\ &= \mu_c k_W g(s-1)\rho d_p^3 \left(cos\alpha - \tfrac{sin\alpha}{\mu_c} + \tfrac{F_C}{F_W}\right) \end{aligned} \tag{28}$$

where k_W, $k_{D,1}$,$k_{D,2}$,k_L all are the constant factors of forces' expressions and the particle Reynolds number $Re^* = \frac{u_c^* d_p}{\nu}$. For a spherical particle $k_W = \frac{\pi}{6}$. $k_{D,1}$ and$k_{D,2}$ are the drag force factor related to particle shape and the factor characterizing the burying of the particle with respect to the mean height of sediment bed respectively. k_L is the factor coupling the lift force coefficient.

Rearrange the above force balance Eq. (28):

$$\frac{u^2 Re^{*2}}{g(s-1)d_p^3} = \frac{\mu_c k_W}{k_{D,1}\left(1 + k_{D,2}Re^{*2}\right) + \mu_c k_L Re^*}\left(cos\alpha - \frac{sin\alpha}{\mu_c} + \frac{F_C}{F_W}\right) \tag{29}$$

Substituting the critical shear stress $\tau_c = \rho u_c^{*2}$ and the particle Reynolds number $Re^* = \frac{u_c^* d_p}{\nu}$ into the definition of critical Shields parameter:

$$\tau_c^* = \frac{\tau_c}{g\rho(s-1)d_p} = \frac{u^2 Re^{*2}}{g(s-1)d_p^3} \tag{30}$$

Hence, comparing with the rearranged force balance Eq. (29), the critical Shields parameter:

$$\tau_c^* = \frac{\mu_c k_W}{k_{D,1}\left(1 + k_{D,2}Re^{*2}\right) + \mu_c k_L Re^*}\left(cos\alpha - \frac{sin\alpha}{\mu_c} + \frac{F_C}{F_W}\right) \tag{31}$$

For the horizontal surface and non-cohesive particles, namely $\left(cos\alpha \quad \frac{sin\alpha}{\mu_c} + \frac{F_C}{F_W}\right) = 1$, the dimensionless critical shear stress for horizontal non-cohesive particle bed is:

$$\tau_{c,o}^* = \frac{\mu_c k_W}{k_{D,1}\left(1 + k_{D,2}Re^{*2}\right) + \mu_c k_L Re^*} \tag{32}$$

which is exactly the same expression in reference (Ternat et al., 2008, Eq. (20)). However, the empirical expression (Guo, 2002) of $\tau_{c,o}^*$ is adopted in AULA as well as quoted in (Weber et al., 2015). In order to avoid determining the related constants, we don't directly use the derived $\tau_{c,o}^*$ Eq. (32). On the contrary, we prefer to apply the empirical correlation of $\tau_{c,o}^*$ Eq. (6), since the empirical expression of $\tau_{c,o}^*$ is validated widely against experimental data (Guo, 2002).

Therefore, we propose a factor to correct the dimensionless critical shear stress, which can be rewritten in a short form as shown in Eq. (10), where the correction factor of inclination and cohesion is:

$$C_{i,c} = \left(cos\alpha - \frac{sin\alpha}{\mu_c} + \frac{F_c}{F_w}\right) \tag{33}$$

3.2.2. Inclination effect

In the case of non-cohesive particles (or the particle size is very large, the cohesive force can be neglected comparing with buoyant weight), the modification of dimensionless critical shear stress with the consideration of inclination but without cohesion is:

$$\tau_c^* = \tau_{c,o}^* \left(cos\alpha - \frac{sin\alpha}{\mu_c} \right) \tag{34}$$

which is consistent with the result in literature (Dey and Papanicolaou, 2008). Since the cohesive force is ignored, which means that all particles balance by the gravitational force, the friction, the lift force, and the drag force. When it comes to a critical case: the inclination angle is larger than the threshold angle α_c, the particle will slide downwards automatically even without the driving of drag force. The Coulomb friction coefficient of natural sediments is recommended as $\mu_c = 0.58 \quad 0.84$. The mean value $\mu_c = 0.7$ and we know the friction coefficient $\mu_c = tan\alpha_c$, hence we estimate the critical inclination angle of natural sediments $\alpha_c = 35^{\circ}$.

The result of inclination correction factor $\left(cos\alpha \quad \frac{sin\alpha}{\mu_c} \right)$ is shown in Fig. 4. The inclination correction factor decreases with the inclination angle increasing. When $\left(cos\alpha \quad \frac{sin\alpha}{\mu_c} \right) = 0$, the inclination reaches its threshold angle. That means the particle will move downwards even without the drag force of flow. If the inclination increase further, the $\left(cos\alpha \quad \frac{sin\alpha}{\mu_c} \right)$ decrease from positive to negative value, which means the driving force is always beyond the resistance. The particles slide downwards automatically if there is no cohesion to compensate.

If the inclination already exceeds its critical angle α_c, but the force ratio $\frac{F_C}{F_W} \geq \frac{sin\alpha}{\mu_c} \quad cos\alpha$, then the particles can also be still on the surface. In this case, we can determine the requirements of particle properties (such as minimum particle size and porosity) based on the known inclination angle.

3.2.3. Cohesion effect

The nuclear aerosols deposited on walls are with very various and complicated components, size distribution, porosity, etc. In the THAI-AW3-LAB experiments, the aerosols can be loaded on vertical walls and then stick there. Accordingly, the cohesive force acting on particles cannot be ignored. Otherwise, when the gravitational force overcome the friction, the particles would slide downwards naturally, and the aerosol erosion rate would be infinite without considering cohesive force additionally. The consequence of the cohesion effect increase the velocity needed for initiation of particle movement. An additional friction comes out when cohesive force is considered in the force balance.

THAI-AW3-LAB experiment reports that the bulk density of silver aerosol is 1100 kg/m^3. The bulk density of silver powder is the ratio of the weight of silver powder to the volume of both silver particles and the void space between the silver particles. The silver material density is 10,490 kg/m^3. The silver material density isn't mentioned in THAI-AW3-LAB report actually, but mentioned in the report of the companion experiment THAI-AW3 (part 1) (Freitag, 2016). Therefore, the silver porosity n can be calculated as:

$$n = 1 - \frac{bulk\ density}{material\ density} \tag{35}$$

So $n = 1 \quad \frac{1100}{10490} \cong 0.9$. The particle porosity is high, namely the particle compactness is low. According to the opinion of (Ternat et al., 2008), the cohesive force of particles with high porosity can be assumed as the interaction between the same size particles, without the influence of the size distribution. The expression of cohesive force is:

$$F_C = \frac{A_H(1 - cos\alpha_c)}{48K(n)^2 d_p} \tag{36}$$

where $A_H \cong 10^{-20}$ Joule is the Hamaker constant. α_c is the critical inclination angle, whose tangent is the coefficient of sliding friction. The compaction function $K(n)$ can be defined by:

$$K(n) = \left(\frac{n_{max} - n_{min}}{n_{max} - n} \right)^{\frac{1}{3}} - 1 \tag{37}$$

where n is the local porosity of particles. In practice the maximum porosity $n_{max} = 1$. The minimum porosity n_{min} depends on the compact structure (namely the packing arrangement as a cubic, hexagonal, or other structures). In our case we prefer the cubic compact structure, due to the low compactness of silver particles, which presents $n_{min} = 1 \quad \frac{\pi}{6}$.

Based on the expressions of cohesive force Eq. (36) and buoyant weight Eq. (25), the curves of the force ratio $\frac{F_C}{F_W}$, as shown in Fig. 5, are plotted against particle size with different porosity n. The boundary condition is in Table 3. Here we take the bulk density as the effective particle density ρ_p.

Fig. 5 reveals that increasing the porosity leads to the decrease of cohesive force obviously. The mean particle diameter used in THAI-AW3-LAB experiments are in the size range 0.7–2.5 μm. In most cases, the cohesive force is comparable to the buoyant weight. The cohesive force can be neglected if particle size is quite big.

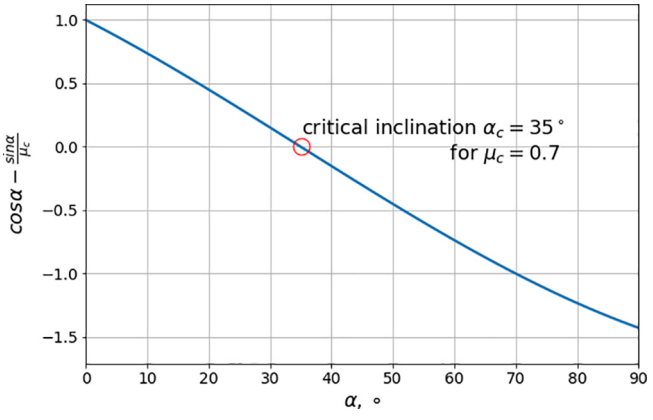

Fig. 4. Inclination correction factor versus the inclination angle.

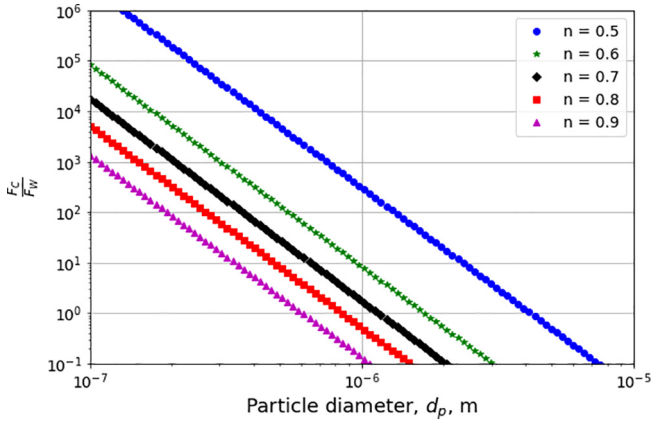

Fig. 5. Force ratio $\frac{F_C}{F_W}$ versus particle size with different porosities.

Table 3
Parameters for the cohesive force modeling.

ρ_p, kg/m^3	ρ, kg/m^3	g, m/s^2	n_{max}	n_{min}	A_H, Joule	$a_{c,}^{\circ}$	k_w
1100	1000	9.8	1	1 $\frac{\pi}{6}$	10 ^{20}	35	$\frac{\pi}{6}$

However, when the porosity$n = 0.9$, the cohesive force is less than the buoyant weight for the experimental particle size in THAI-AW3-LAB. But partial particles are still on vertical walls in THAI-AW3 experiment. It is possible that the porosity is overestimated. The bulk density of silver powder is quite smaller than the silver material density. It is likely that the bulk density would be larger in reality. The larger bulk density is, the more compact the silver particles are. That leads to the smaller porosity n and larger cohesive force accordingly. Another reason is the diameter of the deposited aerosols on vertical walls could be smaller than the mean particle size, since the particle size has a log-normal distribution. The small particles (less than the average size) with high cohesion can be still on the wall with a high inclination angle.

4. Model validation

After coupling the condensate coverage empirical correlation and the proposed correction factor of inclination and cohesion into the aerosol wash-down model AULA, this extended model is validated by the THAI-AW3-LAB experiment as follows.

4.1. THAI-AW3-LAB experiment

Since 1998 the technical-scale test facility **THAI** (**T**hermal-hydraulics, **H**ydrogen, **A**erosols, **I**odine) has been operated by Becker Technologies at Eschborn, Germany, in close cooperation with AREVA and GRS, in order to provide an experimental database for the development and validation of lumped parameter and CFD containment codes. Up to now, at least 6 types of experiments have been performed evaluating the phenomena in containment, such as helium/hydrogen material scaling (HM), hydrogen deflagration (HD), hydrogen recombiner (HR), passive autocatalytic recombiner poisoning, aerosol wash-down, iodine behavior, etc. The experiments of THAI project are designed to fill these knowledge gaps by delivering data for the evaluation of the hydrogen and fission product behavior, thereby supporting the validation of accident simulation codes. In addition, an analytical workgroup was established in the frame of the THAI project, which aimed at the evaluation of the test results for further development and validation of the predictive capabilities of advanced lumped parameter codes and CFD codes currently used in the reactor safety field.

Aerosol wash-down process determines the fission product distribution, which affects the thermal-hydraulics of the containment atmosphere because of the decay heat released by the fission products. Therefore, a serial of aerosol wash-down experiments including THAI-AW, AW2, AW3, and AW4 is carried out in THAI project. The aerosol wash-down experiments have been performed to investigate the aerosol wash-down behavior of insoluble/soluble aerosols on surfaces and the water spray effect. As a first step, THAI-AW addresses the main phenomenon related to the wash-down process of soluble aerosol under superheated thermal–hydraulic conditions. The test phases are defined in a way so that the steam condenses on the vertical vessel walls and further contribute in wash-down of the aerosol deposited on the surfaces. The accumulated condensate is continuously drained into the independent gutters. The test contributes the general knowledge of aerosol wash-down behavior over quasi-horizontal surfaces and small puddles in containment. THAI-AW experiment concludes that the time range of aerosol wash-down is from minutes to hours and the completeness of aerosol wash-down is dependent on water flow rate, aerosol surface load, and the surface characteristics. THAI-AW2 has been performed to investigate the wash-down behaviour of soluble CsI and insoluble SnO_2 aerosols, which concludes the wash-down efficiencies are independent from each other. Soluble aerosol was injected by two nozzles from top of the vessel into the air atmosphere while insoluble aerosol produced by a brushing device was released at the same time also from top of the vessel together with a carrier gas. THAI-AW3 has been conducted in two parts (insoluble aerosol Ag wash-down and the interaction between Ag and iodine in water sump). The insoluble aerosol Ag wash-down on vertical walls, quasi-horizontal surfaces and small puddles by the condensate water flow has been investigated. THAI-AW4 presented the reduction of aerosol concentration in THAI facility by a spray system that is typical for reactor containments. The evolution of aerosol concentration and containment thermal-hydraulics have been investigated.

THAI-AW3-LAB experiment is also one of the aerosol wash-down experiments conducted by Becker Technologies (Laufenberg et al., 2014a,b; Gupta, 2015). It is a laboratory scale test developed and constructed in order to measure the removal of insoluble silver aerosol deposited on inclined surfaces by water flow. The experimental setup is used to perform a series of wash-down tests, in which surface inclination, water flow rate, aerosol load as well as particle sizes are varied. Two different surfaces types (stainless steel and decontamination paint) of interest are representative for containment structures. The test plates are made out of stainless steel and some of them are coated by decontamination paint. A total of 15 tests are conducted. Each test consists of an initial dry aerosol loading phase and the later wash-down phase. The experimental data exhibit a clear trend of a fast aerosol wash-down in the beginning, which is followed by a slow removal transient. Some of tests (such as test 3, test 4, and test 12) can also be used to validate the rivulet behavior and its coverage. The setup consists of trapezoidal inclined plates loaded with insoluble silver aerosol. At the uppermost edge purified water is applied on the plate by a water distributor with a given mass flow rate. A tubular distributor (with 38 holes of 0.7 mm diameter along the edge) is used to generate a homogeneous water distribution. Pictures of the water flow are recorded during the tests, as shown in Fig. 6. These images are used to identify the wetting area of the plates as well as the rivulet behavior. For further information, THAI-AW3-LAB laboratory experiments report (Laufenberg et al., 2014a,b) is recommended.

The surface inclinations of test 3, 4, and 12 are 2°, 20°, and 10° respectively. These tests are conducted under ambient pressure and temperature (25 °C, 1.0 Bar). The mass flow rate is the same, 11 g/s. All test plates have the same structure size. The trapezoidal plate upper width is 0.475 m, the lower width is 0.09 m, and the length is 1.215 m. So the average $Re = \frac{4\rho\dot{V}}{\mu} = 175$. The surface of test 3 and 4 are stainless steel coating with GEHOPON paint, while the test 12 without any paint. The water on GEHOPON paint has a static equilibrium contact angle 60–65°; here we take the average 62.5°. The parameters of THAI-AW3-LAB are summarized in Table 4. In the experiments, the particles are collected in intervals of 10 s for a total duration of 130 s. The aerosol washed down by rivulet is recorded in each 10 s. The effective particle density is used in the aerosol wash-down calculations, because aerosol in containment is usually surrounded by water. The effective particle

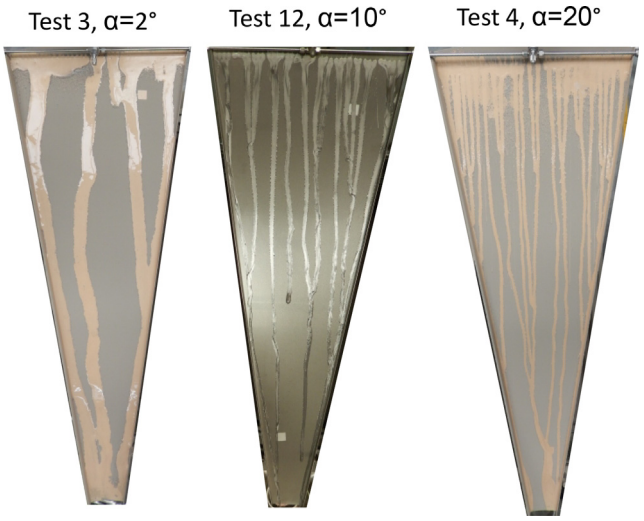

Fig. 6. Rivulet with different inclination in THAI-AW3-LAB (Laufenberg et al., 2014a,b).

density can be roughly determined in the range of the aerosol bulk density and the aerosol density with water fully filled the void space (which numerically is the aerosol bulk density plus the product of water density and aerosol porosity, namely, 1100 kg/m^3 + 0.9 * 1000 kg/m^3 = 2000 kg/m^3). The mean effective particle density 1550 kg/m^3 is adopted in the current simulation of THAI-AW3-LAB.

4.2. Comparison with experimental data

4.2.1. Rivulet behavior

Table 5 reveals the comparison of the rivulet average thickness, velocity, and the coverage. The average value at 130 sec of each THAI-AW3-LAB test are selected. However, for the test 12, we only have data at 900 sec from the experiment report (Laufenberg et al., 2014a,b). Both the experiment and calculation reveal that the average rivulet thickness decrease with the inclination increasing, on the contrary, the average rivulet velocity increase. The results are consistent with the rivulet thickness and velocity model, which are both in terms of inclination angle, roughly $\delta \propto sin\alpha^{-0.4}$ and $u \propto sin\alpha^{0.2}$ (Eq. (17) and Eq. (18)) if *Re*, contact angle, and water propoties keep constant.

The coverage comparison in Table 5 shows the prediction by the empirical correlation increases slightly with inclination angle increasing. The prediction result is consistent with the coverage model, roughly $\varepsilon \propto sin\alpha^{0.2}$ (Eq. (21)), when *Re*, contact angle, and water properties keep constant. The inclination effect is not significant beyond a certain value (e.g. $\alpha > 30^{\circ}$).

However, the experimental data show that the inclination angle doesn't impact the coverage very much, although the inclination angles are small. Perhaps the surface after the aerosol deposition cannot be homogeneous completely (Laufenberg et al., 2014a,b), so that the contact angles would differ from place to place.

Another issue of interest is about the width of individual rivulets and the amount of rivulets in each test, as shown in Fig. 6. It is clear that the amount of rivulets increases with the inclination, while the width of each individual rivulet decrease. We think it is related to the rivulet formation. At beginning, the surface is dry. The water comes out at the uppermost edge with a uniform water injection distribution. The rivulets can flow downwards when the rivulet front can overcome the resistance at front contact line. In addition, we know that the larger rivulet velocity is, the larger dynamic contact angle at the rivulet front is, which leads to a smaller resistance. In other word, the rivulet with larger velocity is easier to move downwards. The rivulets in test 4 have the largest velocity (because of the highest inclination) that the rivulet amount is the most, while the rivulet formation in test 3 needs more water to come together so that the rivulet has an enough large velocity to overcome the resistance.

4.2.2. Aerosol wash-down mass

The aerosol wash-down rate comparisons against THAI-AW3-LAB experiments (test 3, 4, and 12) are shown in Fig. 7, Fig. 8, and Fig. 9 with the erosion constant ($k_{e,0}$ in Eq. (2)) 0.4, 0.005, and 0.03 respectively. The erosion constant has to be estimated and is different from case to case, which depends on the used properties of surface, aerosol, fluid and the wash-down situation (Weber et al., 2015; Amend et al., 2018). All the computational conditions are described in Section 4.1 except the rivulet coverage, which is calculated by the proposed correlation, as shown in Section 4.2.1.

The comparison results generally show good agreements with experimental data, but still have the deviations. In the later phase (from 60 to 130 s), the prediction of aerosol wash-down is lower than the experiment. The aerosol wash-down rate is somehow

Table 4
Parameters of THAI-AW3-LAB.

		Test 3	Test 4	Test 12
Aerosol surface load		26.4 g/m^2	27 g/m^2	10.2 g/m^2
Surface inclination		2°	20°	10°
Surface of plate		Decontamination paint on steel	Decontamination paint on steel	Steel without decontamination paint
Mass flow rate		11 g/s	11 g/s	11 g/s
Particle diameter		1.5–2.5 μm	1.5–2.5 μm	0.7–1.2 μm
Effective particle density		1100–2000 kg/m^3	1100–2000 kg/m^3	1100–2000 kg/m^3
Coverage	At 130 sec	42.8%	44.5%	–
	At 900 sec	45.6%	44.9%	41.7%

Table 5
Rivulet parameters comparison with THAI-AW3-LAB.

	Thickness, mm		Velocity, m/s		Coverage	
	Experiment	Calculation	Experiment	Calculation	Experiment	Calculation
Test 3 - 2°	0.62	1.0	0.137	0.15	42.8%	23.5%
Test 12 -10°	0.41	0.57	0.23	0.21	44.5%	32.5%
Test 4 -20°	0.31	0.43	0.27	0.24	41.7%	37.1%

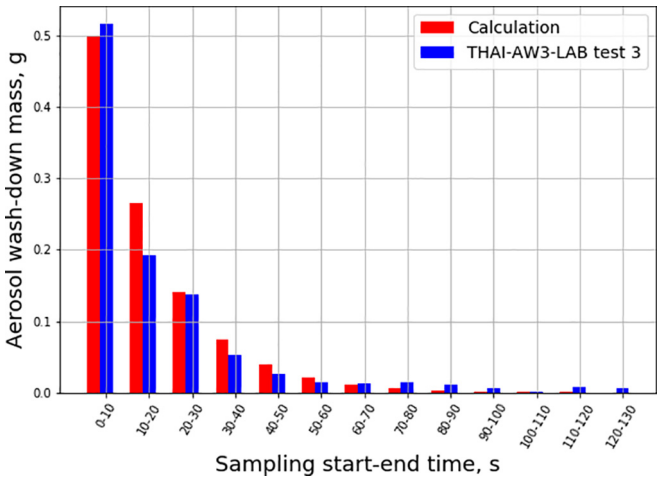

Fig. 7. Aerosol wash-down rate comparing with THAI-AW3-LAB test 3.

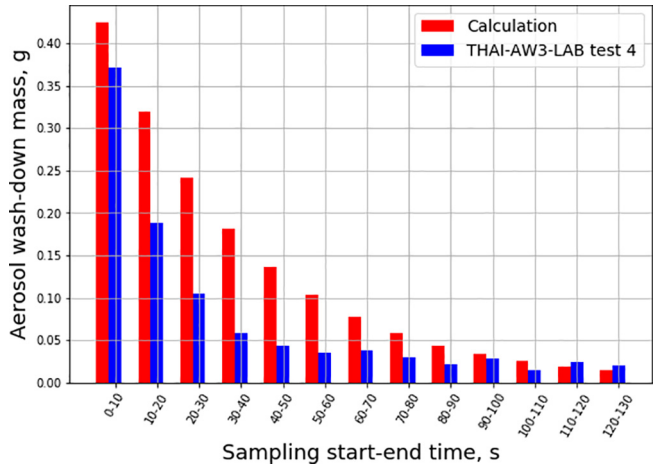

Fig. 8. Aerosol wash-down rate comparing with THAI-AW3-LAB test 4.

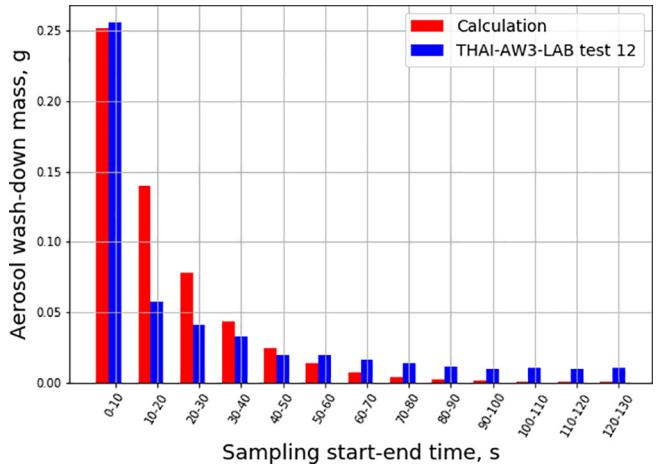

Fig. 9. Aerosol wash-down rate comparing with THAI-AW3-LAB test 12.

linear or constant in the later phase. An explanation is that the rivulet entrains the aerosol along the both edges of each rivulet. The rivulet entrainment is an additional source of the aerosol wash-down rate (Freitag et al., 2018). Nevertheless, in the early 50 s, the deviations are also found. The possible reason is that the rivulet coverage estimation has already about ±25% deviation.

Table 6 shows the comparison of the total aerosol wash-down mass between model prediction and the THAI-AW3-LAB experimental data. The total aerosol mass load on each test plate can be calculated by the aerosol surface density (the aerosol surface load in Table 4) times the plate area. In experiments, the aerosol wash-down efficiency, namely the fraction of the total aerosol wash-down mass (at the end of 130 s) to the total deposited mass is about 10–15%, while in predictions, the efficiency varies from about 11% to 18%. The comparisons reveal there are no significant differences between the calculation and measurement.

5. Model characteristics under severe accident conditions

In this chapter, the extended aerosol wash-down model is applied under a prototypical severe accident condition. The analysis on some parameters of interest, such as particle diameter, density and the surface inclination is carried out. The prototypical conditions are: the pressure of atmosphere and temperature of water are assumed 4 bar and 90 °C respectively (in order to obtain the fluid properties). The static equilibrium contact angles $\theta_e = 62.5A^{\circ}$, which is an experimental measured value for water on a dry containment paint (Inorganic zinc paint) coated stainless steel (Wang and Cheng, 2018). Based on the knowledge of the THAI-AW3-LAB experiment, some other parameters' ranges can be defined, such as, the particle diameter $d_p \in [0.25, 2.5]$, μm, the particle density $\rho_p \in [1100, 3000]$, kg/m^3, and the inclination angle $\alpha \in [2^{\circ}, 90^{\circ}]$. The erosion constant $k_{e,0} = 0.002$, 1/s, the aerosol porosity $n = 0.9$, and the aerosol surface load $c_{ae,0} = 0.027$ kg/m^2. The mass flow rate 0.03 kg/s (should make sure that is a rivulet case, not a fully covered film case). The surface geometry is: wide × high = 1 m × 1 m.

5.1. Particle properties

The particle properties (particle diameter and density) affect the aerosol wash-down threshold very much, since the critical shear velocity is a function of particle properties.

Fig. 10 shows the curves of the critical dimensionless shear stress τ_c^* and critical shear velocity u_c^* versus particle diameter under the prototypical accident conditions and $\rho_p = 1550\, kg/m^3$, $\alpha = 30^{\circ}$ specifically. Both τ_c^* and u_c^* decrease rapidly with particle diameter increasing, where the particle diameter is less than 1 μm. The τ_c^* and u_c^* are keep almost flat while the particle diameter increase further (larger than 1 μm). That is because the cohesive force increase exponentially with the particle diameter decreasing when the particle diameter is less 1 μm, as shown in Fig. 5. The cohesive force dominates the resistance. Consequently, the remaining deposited aerosol mass on the water-covered wall m_{ae} with respect to different particle diameters, as shown in Fig. 11, reveals that time needs longer to wash down the aerosols completely for the particles with smaller diameter due to their larger τ_c^* and u_c^*.

Similarly, Fig. 12 shows the curves of τ_c^* and u_c^* versus particle density ρ_p under the prototypical accident conditions and $d_p = 1$ μm, $\alpha = 30^{\circ}$ specifically. τ_c^* decreases slightly with particle density increasing comparing the decreasing amplitude in Fig. 10, on the contrary, u_c^* increases parabolically with the particle density increasing. As a result, the aerosol wash-down process is stronger with respect to a smaller particle density, as shown in Fig. 13.

5.2. Surface inclination

The inclination impact on aerosol wash-down are not only the critical shear velocity u_c^* as well as the particle properties influence,

Table 6
Total aerosol wash-down mass comparing with THAI-AW3-LAB.

	Test 3		Test 4		Test 12	
	Experiment	Calculation	Experiment	Calculation	Experiment	Calculation
Total mass load	9.1		9.3		3.5	
Total mass wash-down	1.0	1.06	0.98	1.67	0.51	0.56
Efficiency	11.04%	11.6%	10.54%	17.9%	14.48%	16%

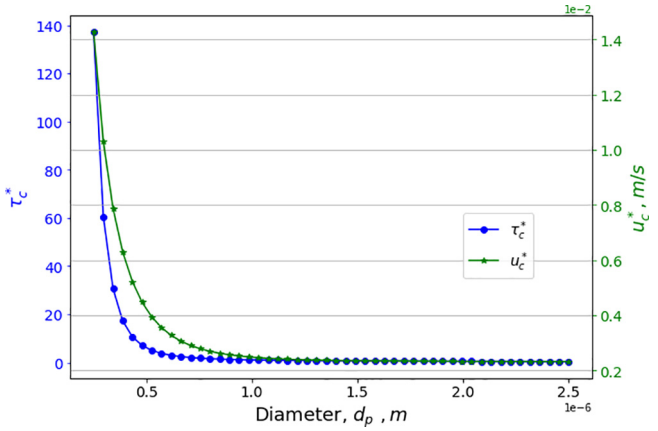

Fig. 10. Critical dimensionless shear stress and critical shear velocity versus particle diameter.

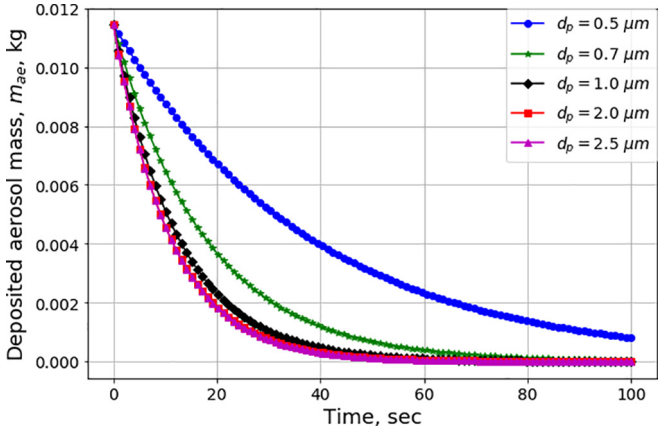

Fig. 11. Remaining deposited aerosol mass over time with different particle diameters.

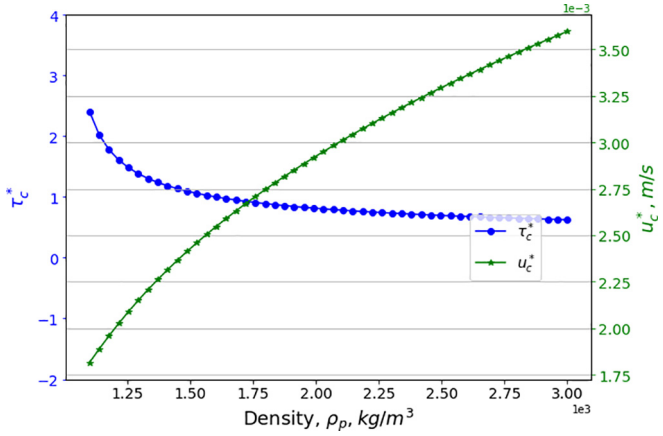

Fig. 12. Critical dimensionless shear stress and critical shear velocity versus particle density.

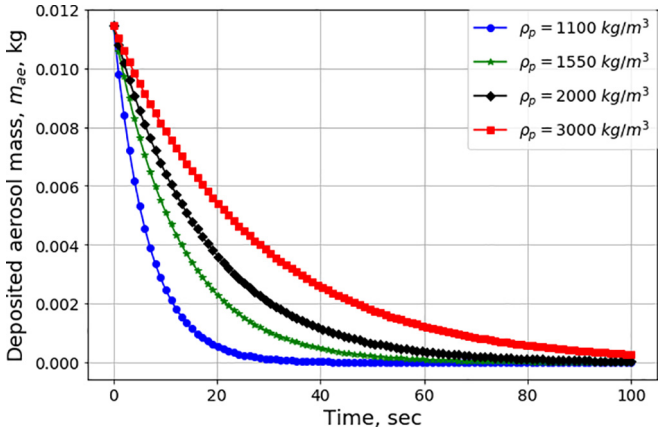

Fig. 13. Remaining deposited aerosol mass over time with different particle densities.

but also the rivulet shear velocity u^*. Fig. 14 shows the variation of both u_c^* and u^* with the inclination increasing under the prototypical accident conditions and $\rho_p = 1550\ \mathrm{kg/m^3}$. The rivulet shear velocity increases with inclination, since the rivulet model tells the rivulet velocity is proportional to $sin\alpha^{0.2}$, and the rivulet shear velocity has the same monotonicity as rivulet velocity. However, the critical shear velocity u_c^* decreases with the inclination increasing, because of the negative inclination effect, as we discussed in Section 3.2.2. Accordingly, it's possible to find the cross point between the two curves for a specific particle diameter, for instance as shown in Fig. 14, the intersection between the blue dot curve and the green star one. That means there is no aerosol wash-down when the inclination is less than the cross point (~20° for the current case). Consequently, the erosion rate equals zero, as shown in Fig. 15.

Moreover, we can also define the boundary of the particle diameter. As shown in Fig. 14, no matter how large the inclination is, if the particle diameter is less than 0.21 μm, there is no wash-down

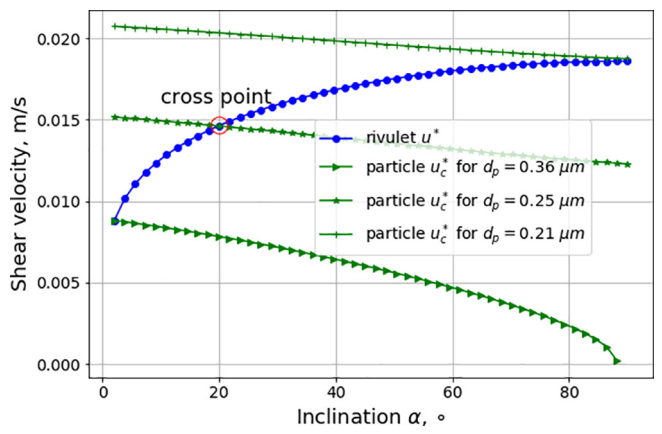

Fig. 14. Surface inclination impact on shear velocity.

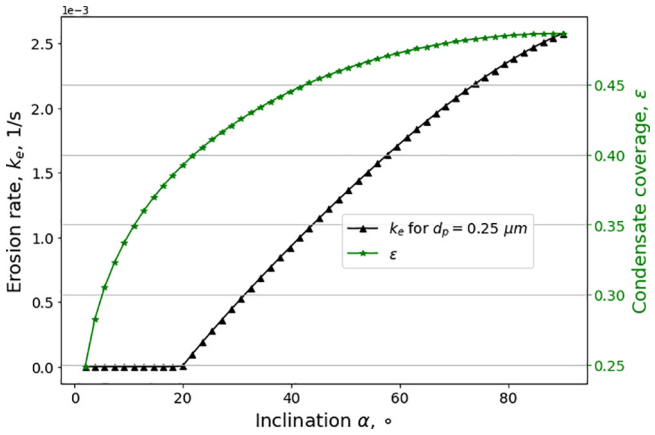

Fig. 15. Erosion rate and condensate coverage versus inclination.

any more, while if the particle diameter is larger than 0.36 μm there is always wash-down under the current prototypical accident conditions.

Fig. 15 also indicates the rivulet coverage and the erosion rate increase with the surface inclination, as a result, the aerosol wash-down efficiency also increases with inclination angle.

6. Conclusions

The aerosol wash-down process is significant to evaluate radiative source term distribution in nuclear containment. The work presented aims at improving the already existing aerosol wash-down model AULA. It is extended by estimation of rivulet coverage and consideration of surface inclination and aerosol cohesion. The extended aerosol wash-down model is validated by THAI-AW3-LAB experiment.

The estimation of rivulet coverage is a necessary boundary condition for calculating aerosol wash-down. A new empirical correlation of coverage is proposed. The validation against the experimental data indicates a good agreement with around ±25% deviation. Uncertainties of rivulet behavior have to be discussed further. The coverage correlation is eventually coupled to calculate the aerosol wash-down process.

In order to improve the dimensionless critical shear stress model, a correction factor is deduced by force analysis, which considers the wall inclination and aerosol cohesion. The critical shear stress decreases with the increase of inclination. The cohesive force depends on the particle diameter and porosity. The smaller diameter and porosity leads to a lager cohesion.

The extended aerosol wash-down model with the consideration of inclination and cohesion is validated by the THAI-AW3-LAB experiment. The comparison results show generally good agreements, although the uncertainties of rivulet formation and coverage are large. The improved critical Shields parameter considering the inclination and cohesion is feasible to assess the erosion threshold of aerosol wash-down.

Furthermore, the model characteristics under severe accident conditions and the analysis on aerosol density, diameter, and inclination are presented and discussed. The results show the smaller density and lager diameter have a higher aerosol wash-down efficiency. The inclination impact not only on the critical shear velocity but also the rivulet shear velocity.

Next step, the containment program COCOSYS will be used to simulate the integral aerosol wash-down experiment THAI-AW3 for a further validation. We are also going to apply the model in a generic containment in order to investigate the influence of severe accident scenarios. It is worth noting that, under different severe accident scenarios, the terms of Ka and Re number in rivulet coverage model are strongly influenced by containment thermal-hydraulics. The aerosol injection and deposition, as well as wash-down process accordingly, are affected by core degradation process and molten core-concrete interaction. All parameters related to wash-down model can be updated for each time step in the containment code COCOSYS.

CRediT authorship contribution statement

Fangnian Wang: Conceptualization, Writing - original draft. **Xu Cheng:** Supervision, Writing - review & editing.

Declaration of Competing Interest

The authors declare that they have no known competing financial interests or personal relationships that could have appeared to influence the work reported in this paper.

Acknowledgments

This work is supported by the project "Erweiterung des Strömungsmodells zur Simulation des Aerosolabwaschens (ESSA, grant number:1501537)", funded by the German Federal Ministry of Economic Affairs and Energy(BMWi). We thank our partners Holger Norwack, Sara Beck from GRS and Sanjeev Gupta from Becker Technologies for many fruitful discussions and experimental data support. I also thank the financial support from China Scholarship Council (CSC, China, File Number: 201709110142).

Reference

Amend, K., Klein, M., München, U.D.B., Weg, W.H., 2018. Modeling and simulation of water flow on containment walls with inhomogeneous contact angle distribution. ATW Int. J. Nucl. Power 62 (7), 477–481.
Ariathurai, R., 1977. Mathematical Model of Estuarial Sediment Transportation PhD thesis. University of California.
Ausner, I., 2007. Experimentelle Untersuchungen mehrphasiger Filmströmungen. PhD Thesis.
Bridgman, P.W., 1931. Dimensional analysis. Yale University Press, New Haven, CT.
Buckingham, E., 1914. On physically similar systems; illustrations of the use of dimensional equations. Phys. Rev. 4 (4), 345.
Dey, S., Papanicolaou, A., 2008. Sediment threshold under stream flow: a state-of-the-art review. KSCE J. Civil Eng. 12 (1), 45–60.
Doniec, A., 1988. Flow of a laminar liquid film down a vertical surface. Chem. Eng. Sci. 43 (4), 847–854.
Doniec, A., 1991. Laminar flow of a liquid rivulet down a vertical solid surface. Can. J. Chem. Eng. 69 (1), 198–202.
Dupont, J., 2017. Thin liquid film dynamics in a condensing and re-evaporating environment. Phys. World. https://doi.org/10.1088/2058-7058/7/6/30.
El-Genk, M.S., Saber, H.H., 2001. Minimum thickness of a flowing down liquid film on a vertical surface. Int. J. Heat Mass Transf. 44, 2809–2825. https://doi.org/10.1016/S0017-9310(00)00326-4.
Freitag, M., 2016, Wash-Down Behavior of Silver Aerosols Test AW-3 (Part 1). 1501455-TR-AW-3 (Part 1), Becker Technologies (Jan. 2016).
Freitag, M., Gupta, S., Beck, S., Sonnenkalb, M., 2018. Experimental and analytical investigations of aerosol processes—wash-out and wash-down. Nucl. Sci. Eng. 193, 198–210. https://doi.org/10.1080/00295639.2018.1479091.
Guo, J., 2002. Hunter rouse and shields diagram. Adv. Hydraul. Water Eng. 2, 1096–1098. https://doi.org/10.1142/9789812776969_0200.
Gupta, S., Langer. G, 2009. Aerosol Wash-down Test (AW), OECD-NEA THAI Project , Report No. 1501326–AW-QLR, Becker Technologies, December 2009.
Gupta, S. et al., 2012. Wash-down Behaviour of Soluble and Non-soluble Aerosols Test ID: AW-2. Report No. 1501361-TR-AW-2. Becker Technologies.
Gupta, S., 2015. THAI experiments on volatility, distribution and transport behaviour of iodine and fission products in the containment. Proceedings of the International OECD-NEA/NUGENIA-SARNET Workshop on the Progress in Iodine Behaviour for NPP Accident Analysis and Management.

Hartley, D.E., Murgatroyd, W., 1964. Criteria for the break-up of thin liquid layers flowing isothermally over solid surfaces. Int J Heat Mass Transfer 7 (9), 1003–1015.
Hillebrand, G., 2008. Transportverhalten kohäsiver Sedimente in turbulenten Strömungen (Doctoral dissertation, KIT-Bibliothek). Untersuchungen im offenen Kreisgerinne.
Hobler, T., 1964. Minimum surface wetting (in Polish). Chemia Stosow. 2B, 145.
Hoehne, M., Weber, G., 2010. Interpretation of the OECD THAI CsI Aerosol Wash-down Test AW by COCOSYS analyses. OECD THAI Seminar, Paris, 6 and 7 Oct., 2010.
Huang, X., Cheng, X., 2015. Modification and application of water film model in COCOSYS for PWR's passive containment cooling. Nucl. Eng. Des. 280, 251–261. https://doi.org/10.1016/j.nucengdes.2014.08.026.
Klein-Heßling, W., Arndt, S., Weber, G., Nowack, H., Spengler, C., Schwarz, S., Pelzer, M., Eckel, J., 2015. COCOSYS v2.4 User's Manual. GRS.
Laufenberg, B. Von, Colombet, M., Freitag, M., 2014. Wash-down Tests of Silver Aerosol from Stainless Steel and Painted Surfaces. NUTHOS-10, Okinawa, Japan, December 14–18.
Laufenberg, B. Von, Colombet, M., Freitag, M., 2014. Wash-Down of Insoluble Aerosols: Results of the Laboratory Tests Related to THAI AW-3 Test, 1501455-TR-AW-3-LAB, Becker Technologies, July 2014.
Nusselt, W., 1916. Die Oberfleachenkondensation des Wasserdampfes. VDI-Zeitschr. 60 (27), 541–546.
Shields, A., 1936. Anwendung der Aehnlichkeitsmechanik und der Turbulenzforschung auf die Geschiebebewegung PhD Thesis. Technical University Berlin.
Ternat, F., Boyer, P., Anselmet, F., Amielh, M., 2008. Erosion threshold of saturated natural cohesive sediments: Modeling and experiments. Water Resour. Res. 44 (11).
Wang, F., Cheng, X., 2018. Model assessment of condensate droplet motion on inclined containment structure surface. NUTHOS-12 1–13.
Wang, F., Cheng, X., 2019. Modeling approach of flowing condensate coverage rate on inclined wall for aerosol wash-down. Nucl. Eng. Des. 355, (2019) 110349.
Weber, G., 2011. Ein neues Abwaschmodell für unlösliche Aerosole (AULA), GRS-TN-WEG-01/2011, Aug.
Weber, G., Funke, F., Gupta, S., 2015. Iodine and Silver Wash-Down Modelling in Cocosys-Aim By Use of Thai Results. OECDNEA/NUGENIA-SARNET Work.
Yu, Y.Q., Wei, S.J., Yang, Y.H., Cheng, X., 2012. Experimental study of water film falling and spreading on a large vertical plate. Prog. Nucl. Energy 54, 22–28. https://doi.org/10.1016/j.pnucene.2011.09.007.